PAPER

Influence of interparticle friction on the magneto-rheological effect for magnetic fluid: a simulation investigation

IOP Publishing Smart Materials and Structures
Smart Mater. Struct. **29** (2020) 115002 (10pp) https://doi.org/10.1088/1361-665X/ababe3

Influence of interparticle friction on the magneto-rheological effect for magnetic fluid: a simulation investigation

Lei Pei[1], Shouhu Xuan[1,2], Haoming Pang[1] and Xinglong Gong[1]

[1] CAS Key Laboratory of Mechanical Behavior and Design of Materials, CAS Center for Excellence in Complex System Mechanics, Department of Modern Mechanics, University of Science and Technology of China, Hefei 230027, People's Republic of China
[2] National Synchrotron Radiation Laboratory, University of Science and Technology of China, Hefei 230027, People's Republic of China

E-mail: xuansh@ustc.edu.cn and gongxl@ustc.edu.cn

Received 14 April 2020, revised 18 July 2020
Accepted for publication 2 August 2020
Published 21 September 2020

Abstract

This work studied the effect of interparticle friction force on the magnetorheological properties for magnetic fluid using particle-level dynamic simulations. A novel numerical model considering the friction force and elastic normal force between coarse microspheres was developed. The analysis revealed the relationship between magnetic fluid microstructure and friction coefficient (μ) of particles for the first time. Under steady shear flow, plate-like aggregations were formed under a moderate friction coefficient ($\mu \approx 0.2$), while thick chains with large inclinations were observed under strong friction forces ($\mu > 1.5$). When $0.2 \leq \mu \leq 1.5$, the friction forces hardly affected the rheological properties. If $\mu > 1.5$, friction forces could enhance the shear stress by 102%. Friction force hampered the relative movement of magnetic particles in the thick chains and enlarged the average dip angle of microstructures. The magnetic dipolar force between microspheres generated stronger shear stress in such particle aggregations. The optimal friction coefficient was determined as $2 \leq \mu \leq 2.75$ in simulations by considering the saturation magnetizations, external fields, shear rates, and particle concentrations. The enhancement of shear stress was relevant to the relative strength between magnetic force and friction interaction. Simulated shear stress in magnetic field sweep matched well with experiments in the literature. This work will open a promising avenue in the development of high-performance magnetic fluid.

Keywords: magnetic fluid, MR effect, friction force, microstructures, particle-level dynamic simulations

(Some figures may appear in colour only in the online journal)

1. Introduction

Magnetic fluid is a smart material prepared by suspending magnetic particles into a non-magnetic liquid matrix [1]. Carbonyl iron and magnetite were the most conventional magnetic materials due to their high saturation magnetization, super-paramagnetic properties, and easy availability [2, 3]. Under an external magnetic field, particles will attract each other under the action of magnetic dipolar force and aggregate into chain-like or plate-like microstructures. The viscosity and yield stress enormously grow within the order of milliseconds, which is called the magnetorheological (MR) effect [4]. This reversible and controllable mechanical property makes magnetic fluid be widely applied in engineering and biomedical fields, such as dampers, vibration absorbers, magnetic resonance imaging, and magnetic thermal therapy [5–10]. However, sedimentation is always a challenge in the magnetic fluid due to the inherent density mismatch between particle and matrix.

In the past decades, great effort has been devoted to improve the MR effect and overcome the sedimentation at the same time, such as modifying the shape and surface of magnetic particles [11–13]. The MR effect of magnetic fluid depends on the assembled microstructures of dispersed magnetic particles, which is finally dominated by the interparticle forces. The friction force or so-called tangential force greatly influences the particle aggregations and macroscopic mechanical properties [14, 15]. Several novel magnetic fluids based on plate-like and flower-like particles with a large friction coefficient presented excellent MR effect and settlement stability [16, 17]. Porous iron magnetic fluid with rough particle surfaces presented higher storage modulus than solid iron magnetic fluid under a small field [18]. However, the large friction force does not always enhance the MR effect. Siebert's experiments indicated that a higher shear viscosity was achieved by reducing the destructive friction effect in magnetic fluid [19]. The trend of shear stress versus interparticle friction coefficient has not been investigated yet. To develop high-performance magnetic fluid, revealing the effect of interparticle friction on steady shear rheology of magnetic fluid is urgently required.

Simulation has become a powerful tool in developing the mechanism of magnetic fluid due to the merits of low cost and easy to change parameters. Molecular dynamics, particle-level dynamic simulations, finite element method, and computational fluid dynamics have been utilized to explain the experimental results and predict the MR effect [20–23]. Among these numerical methods, particle-level dynamic simulations possess the same time scale and spatial scale with the evolution of microstructures in real magnetic fluid [24]. This method is widely applied to study the rheological behavior of magnetic fluid under different loadings. Ruiz-López *et al* simulated the yield stress of magnetic fluid in shear mode and squeeze mode, which matched well with experiments [25, 26]. The change of mechanical properties were explained by microstructures evolution. However, the interparticle friction force was usually ignored in steady shear simulations of magnetic fluid [27]. It was found that the friction affected the dynamic response of magnetic fluid under oscillatory shear flow [28]. However, only several pre-defined regular microstructures were considered and simulated. The existing theoretical model needs to be further improved to evaluate the complex particle interactions from the point of fundamental research. Based on the above analysis, particle-level dynamic simulation is desirable to study the influence of friction forces on the MR effect of magnetic fluid.

In this work, modified particle-level dynamic simulations were employed to investigate the influence of interparticle friction on the MR effect of magnetic fluid based on general coarse magnetic microspheres. The clarified simulation model considered the friction force and elastic normal force between particles. The microstructures and shear stress of magnetic fluid under the action of interparticle friction forces were obtained. Friction coefficient dependent shear stress under different saturation magnetizations, external field strengths, shear rates, and particle concentrations, was systematically discussed. The optimal friction coefficient was determined. A possible mechanism was developed to explain the relationship between interparticle friction force and MR effect. Finally, the shear stress of Fe_3O_4@SiO_2 magnetic fluid reported in the literature was simulated to verify the accuracy of this work [29]. A quantitative correspondence between simulation and experiment was obtained.

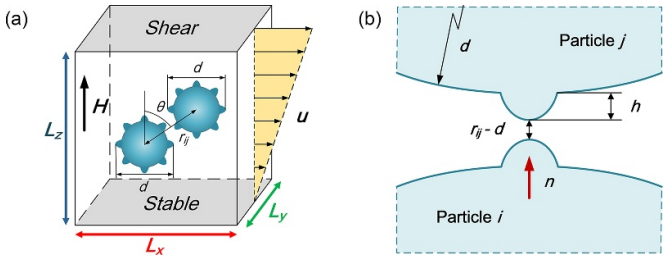

Figure 1. Schematic diagram of (a) the simulation box and (b) small asperities at the surface of coarse magnetic microspheres. The height of asperities was not plotted in scale.

2. Numerical method

2.1. Basic assumptions and conditions

The basic assumptions and set up of simulations are illustrated in this section. Monodisperse coarse magnetic microspheres are randomly distributed in a cubic simulation box at the initial (figure 1(a)). Periodic boundary conditions are adopted on the x-z and y-z planes, while shear boundary conditions are employed on the x-y plane. Then, a uniform magnetic field along the z-direction is applied. The steady shear flow toward the x-direction starts at the same time. Microstructures and shear stress of magnetic fluid keep evolving until homeostasis. The magnetic dipolar force, van der Waals force, elastic extrusion force, friction force, and hydrodynamic viscous force are considered. The gravity, buoyancy, inertia, moment of inertia, and Brownian force are neglected. In typical experiments and applications of magnetic fluid, the driven force of shear flow is much stronger than the particle-matrix interaction. For simplicity, the matrix is assumed in a steady shear flow with a constant shear rate during the simulations.

The roughness of particles can be modeled by a large number of small asperities on the surface (figure 1(b)) [30]. For conventional coarse magnetic microspheres, the typical height of asperities h is usually $10^{-3} \sim 10^{-1}$ of the particle diameter [31]. If a pair of microspheres with a relative tangential velocity are squeezed against each other, the deformation of those asperities will generate a normal extrusion force and a tangential friction force.

2.2. Interparticle forces

The relationship between magnetic moment $\boldsymbol{m}$ and magnetic field strength $\boldsymbol{H}$ can be characterized by the Langevin function [32]:

$$\boldsymbol{m}_i = M_s \left[\coth(x) - \frac{1}{x}\right] V_p \frac{\boldsymbol{H}}{H}, \; x = \frac{M_s V_p H}{k_B T}, \qquad (1)$$

where M_s represents the saturation magnetization. V_p means the average volume of microspheres. k_B and T stand for Boltzmann's constant and absolute temperature, respectively. $H = |\boldsymbol{H}|$. After being magnetized by the external field, each sphere will also generate a magnetic field in the surrounding area. The field strength induced by sphere i at the position of sphere j is:

$$\boldsymbol{H}_i = -\frac{1}{4\pi {r_{ij}}^3}\left[\boldsymbol{m}_i - 3\left(\boldsymbol{m}_i \cdot \hat{\boldsymbol{r}}\right)\hat{\boldsymbol{r}}\right], \tag{2}$$

where r_{ij} indicates the distance between two spheres. $\hat{\boldsymbol{r}}$ is a unit vector from i to j. The total magnetic field strength and magnetic moment of each sphere can be obtained by using the superposition method. According to the point-dipole model, the magnetic dipolar force imposed on sphere i exerted by sphere j is given by:

$$\begin{aligned}\boldsymbol{F}_{ij}^{\mathrm{m}} = \frac{3\mu_0}{4\pi {r_{ij}}^4} c_{\mathrm{m}} \left[\left(-\boldsymbol{m}_i \cdot \boldsymbol{m}_j + 5\boldsymbol{m}_i \cdot \hat{\boldsymbol{r}}\, \boldsymbol{m}_j \cdot \hat{\boldsymbol{r}}\right)\hat{\boldsymbol{r}}\right. \\ \left. - \left(\boldsymbol{m}_i \cdot \hat{\boldsymbol{r}}\right)\boldsymbol{m}_j - \left(\boldsymbol{m}_j \cdot \hat{\boldsymbol{r}}\right)\boldsymbol{m}_i\right].\end{aligned} \tag{3}$$

Here, the magnetic permeability of the matrix is assumed the same as $\mu_0 = 4\pi \times 10^{-7}$ N A^{-2}. θ in degree is defined as the angle between $\hat{\boldsymbol{r}}$ and the external field. c_{m} is the correctional factor to the point-dipole model [33]:

$$c_{\mathrm{m}} = \begin{cases} 1 + \left(3 - \dfrac{2r_{ij}}{d}\right)^2 \left[\dfrac{0.6017}{1 + e^{\frac{(|\theta| - 34.55)}{12.52}}} - 0.2279\right] & r \le 1.5d_{ij} \\ 1 & r > 1.5d_{ij}, \end{cases} \tag{4}$$

where d is the diameter of microspheres. c_{m} only works between neighboring particles. The error of the point-dipole model c_{m}–1 ranges from −23.1% to 33.3%.

The van der Waals force between two microspheres is expressed as [34]:

$$\boldsymbol{F}_{ij}^{\mathrm{vdW}} = \frac{A}{6} R_{ij} d^2 \left[\frac{1}{{R_{ij}}^2 - d^2} - \frac{1}{{R_{ij}}^2}\right]^2 \hat{\boldsymbol{r}}, \tag{5}$$

where $A = 3 \times 10^{-20}$ J is the Hamaker constant [35]. $R_{ij} = \max[r_{ij}, 1.01d]$ [36].

The Hertz contact theory is employed to describe the elastic normal force. If two particles are in contact ($r_{ij} < d$), particle i experiences an extrusion force as [37]:

$$\boldsymbol{F}_{ij}^{\mathrm{n}} = -\frac{2}{3}\frac{E}{1 - \nu^2} h^{\frac{1}{2}} \left(d - r_{ij}\right)^{\frac{3}{2}} \boldsymbol{n}, \tag{6}$$

where $d - r_{ij}$ is the overlap distance between particles. h represents the height of asperities on the surface. E represents the Young modulus and ν stands for the Poisson ratio of the asperities. $\boldsymbol{n}$ is a unit vector outward from particle i.

The interparticle friction force is calculated according to the normal force. Two situations, the stick-phase and slip-phase can be distinguished according to the following criterion [31]:

$$\boldsymbol{F}_{ij}^{\mathrm{t}} = \begin{cases} -\dfrac{2}{7}\dfrac{\left|\boldsymbol{F}_{ij}^{\mathrm{n}}\right|}{d - r_{ij}}\boldsymbol{\delta} & \left|\boldsymbol{F}_{ij}^{\mathrm{t}}\right| < \mu\left|\boldsymbol{F}_{ij}^{\mathrm{n}}\right| \text{ (stick-phase)} \\ \mu\left|\boldsymbol{F}_{ij}^{\mathrm{n}}\right| \dfrac{\boldsymbol{F}_{ij}^{\mathrm{t}}}{\left|\boldsymbol{F}_{ij}^{\mathrm{t}}\right|} & \text{otherwise (slip-phase),} \end{cases} \tag{7}$$

where μ means the friction coefficient. $\boldsymbol{\delta}$ is the relative tangential displacement between two particles during a time step of the simulation. Here the tangential force in the stick-phase is modeled as a linear spring-like force with a threshold. The stiffness of the tangential spring is related to the normal force and finally depends on the overlap distance. It is very difficult to measure the friction coefficient between two microspheres by experiments. Wu and Brizmer *et al* developed the elastic-plastic contact model of spheres and theoretically deduced the value of μ, which was dependent on the normal force [38, 39]. With a decreasing normal force, the friction coefficient increased from $\mu = 0.27$ to $\mu > 1$. This work is principle research on the magnetic fluid based on coarse magnetic particles. To obtain the relationship between shear stress and interparticle friction force, the friction coefficient was considered as different constants in the simulations. The value of μ was set between 0.2 and 3.75 in this work.

2.3. Kinetic equation

In a magnetic fluid, the flow of the matrix around each magnetic particle is a laminar flow with a small Reynolds number. The characteristic length of the flow is the diameter of particles $L = \mathrm{O}(10^{-6}$ m). The characteristic velocity of the flow is the relative velocity between particle and matrix. This value can be determined from the rheological tests as $U = \dot{\gamma}h = \mathrm{O}(10^{-1}$ m s$^{-1})$. Here $h = 1$ mm represents the thickness of the magnetic fluid sample in the rheometer. Finally, the Reynolds number is obtained as $\mathrm{Re} = \rho \mathrm{UL}/\eta = \mathrm{O}(10^{-1})$. $\eta = 10^{-3}$ Pa·s is the viscosity of water. The viscous drag force imposed on a single microsphere is given by:

$$\boldsymbol{F}_i^{\mathrm{d}} = -3\pi\eta d c_{\mathrm{h}} \left(\boldsymbol{v}_i - \boldsymbol{u}_i\right), \tag{8}$$

where $\boldsymbol{v}_i - \boldsymbol{u}_i$ is the relative velocity of particles. c_{h} is a correction factor to the Stokes law for concentrated particle suspensions [40]:

$$c_{\mathrm{h}} = \frac{1 + 5.81\varphi}{\left(1 - \varphi\right)^3} + 0.48\frac{\sqrt[3]{\varphi}}{\left(1 - \varphi\right)^4} + \varphi^3 \mathrm{Re}\left[0.95 + \frac{0.61\varphi^3}{\left(1 - \varphi\right)^2}\right], \tag{9}$$

where φ is the volume fraction of particles. Considering all the aforementioned interactions, the kinetic equation can be concluded as:

$$\sum_{j \neq i}\left(\boldsymbol{F}_{ij}^{\mathrm{m}} + \boldsymbol{F}_{ij}^{\mathrm{vdW}} + \boldsymbol{F}_{ij}^{\mathrm{n}} + \boldsymbol{F}_{ij}^{\mathrm{t}}\right) + \boldsymbol{F}_i^{\mathrm{d}} = 0. \tag{10}$$

In this work, the kinetic equation was solved by using the explicit scheme. The interactions among the particles in the next time step were determined according to the current positions of particles. The velocities of particles in the next time step were calculated from the viscous drag force. For each pair

of particles in contact, the stress component generated by the interparticle normal force and friction force is written as [31]:

$$S_{ij} = \frac{r_{ij}}{2}\left[\left(\boldsymbol{F}_{ij}^{\mathrm{n}} + \boldsymbol{F}_{ij}^{\mathrm{t}}\right)\frac{\hat{\boldsymbol{r}}}{2} + \frac{\hat{\boldsymbol{r}}}{2}\left(\boldsymbol{F}_{ij}^{\mathrm{n}} + \boldsymbol{F}_{ij}^{\mathrm{t}}\right)\right]. \tag{11}$$

The magnetic potential energy U_{m} and magneto-induced stress tensor σ can be written as:

$$U_{\mathrm{m}} = \mu_0\left[\sum_i -\boldsymbol{m}_i\cdot\boldsymbol{H} + \sum_{j>i}\frac{1}{4\pi {r_{ij}}^3}\left(\boldsymbol{m}_i\cdot\boldsymbol{m}_j - 3\boldsymbol{m}_i\cdot\hat{\boldsymbol{r}}\,\boldsymbol{m}_j\cdot\hat{\boldsymbol{r}}\right)\right], \tag{12}$$

$$\sigma = \frac{1}{V}\sum_{j>i}\left[\boldsymbol{r}_{ij}\left(\boldsymbol{F}_{ij}^{\mathrm{m}} + \boldsymbol{F}_{ij}^{\mathrm{vdw}}\right) + S_{ij}\right], \tag{13}$$

where V is the volume of the simulation box.

3. Results and discussion

General coarse magnetic microspheres with different saturation magnetizations were mainly investigated in this work. To verify the accuracy of simulations, shear stress of magnetic fluid based on Fe_3O_4@SiO_2 core–shell microspheres reported by Chae *et al* were finally simulated and compared to experiments [29]. The simulation parameters of two kinds of magnetic particles were chosen as typical experimental values in the literature (table 1) [29, 33, 41–44]. For general coarse micro-spheres, two representative saturation magnetizations (200 and 366 kA m^{-1}) were chosen as samples. The viscosity of the matrix was set as 0.1 Pa s in this work [29].

3.1. Evolution of microstructures and shear stress

To determine the relationship between particle aggregation and rheological property of magnetic fluid based on coarse magnetic microspheres, the microstructures and shear stress in steady shear flow were first simulated. Here, the particle concentration, saturation magnetization, external field, and shear rate were 10 vol%, 200 kA m^{-1}, 34 kA m^{-1}, and 100 s^{-1}. The friction coefficient was set as 0.27 according to the contact theory [38, 39].

The snapshots of microstructures at different moments were plotted in figure 2 by using the OVITO software [45]. The asperities on the surface were so small that particles were still spherical in the micrometer scale. When applying the external field and shear flow, magnetic fluid instantly gained the negative potential energy due to the particle-external field interaction (figure 3(a)). $N \approx 2000$ represented the total number of particles in the simulation. At this time, microspheres still exhibited a chaotic state with a uniform radial distribution function (RDF) of $g(r) \approx 1$ (figure 3(b)). Then, particles rapidly aggregated along the z-axis and formed short single-particle-width chains within 0.5 ms. The magnetic potential energy per particle sharply decreased into a trough. An obvious peak at $r/d = 1$ and three minus peaks at $r/d = 1.7$, 1.9, and 2.5 appeared in the RDF curves. The rest of the curve was very close to zero. The main peak reflected the head-to-tail configuration of particles along the field direction and the others represented the aggregation in the x-y plane. At 2 ms after the start of the simulation, short chains merged into long chains and rotated toward the direction of flow. The decreasing speed of magnetic potential energy slowed down from 1.3×10^{-14} to 7.1×10^{-16} J s^{-1}. Shear stress linearly increased over time until a peak value. This phenomenon was similar to the stress–strain curve of elastic materials before yielding in the quasi-static tensile. The slop was 20.4 Pa ms^{-1} obtained from linear fitting. This phenomenon indicated that magnetic fluid exhibited solid-like properties at the current state. The steady shear flow was not fully developed yet. The dip angle of particle chains showed a great influence on the shear stress. If the angle θ between $\hat{\boldsymbol{r}}$ and the external field was 25°, the magnetic dipolar force gave the maximum contribution to the shear stress [34]. After that, particle chains were destroyed by the flow of the matrix and reconstructed under the magnetic dipolar forces. Thick chain-like aggregations were observed at 10 ms. Shear stress started to fall back and fluctuated around a certain value. The knee point was corresponding to the breakage of microstructures as well as the yield point of magnetic fluid. RDF curves also fluctuated with the destruction and reconstruction of microstructures. The peak values of RDF slightly increased with the development of shear flow, which indicated the microstructures became more and more compact. At 50 ms, thick particle chains evolved into plate-like microstructures parallel to each other. The magnetic potential energy reached a steady-state, which meant the dynamic equilibrium of magnetic fluid. The average shear stress from 25 to 50 ms could represent the macroscopic shear stress of magnetic fluid according to figure 3(a).

According to equation (6), the elastic normal force was in proportion to the three halves power of the overlap distance. Even though the height of asperities was only $h/d \approx 10^{-3} \sim 10^{-1}$, the normal force might grow to a large extent if large deformation appeared between particles. An extremely large normal force would cause the divergence of simulations. According to the literature, an upper limit of the interparticle elastic normal force was set as $\boldsymbol{F}^{\mathrm{n}}{}_{\max} = 10\,\boldsymbol{F}^{\mathrm{m}}{}_{\max}$ to avoid this problem [33, 34, 46]. Here $\boldsymbol{F}^{\mathrm{m}}{}_{\max}$ represented the maximum magnetic dipolar force between a pair of microspheres. The extrusion force would not further increase after reaching this upper limit. The simulated shear stress under different upper limits of elastic normal force was compared in figure 4(a). Here the maximum elastic normal force between particles was set as 5, 10, 15, and 20 times the maximum magnetic dipolar force. The curves were quite close to each other. Both the maximum shear stress and average shear stress exhibited no difference. The upper limit of the normal force did not affect the simulation results. In conventional simulations of magnetic fluid, an exponential repulsive force was usually employed instead of the Hertz contact theory [33, 34]. Similar upper limits were adopted for the repulsive force to ensure the robustness of programs.

Table 1. Simulation parameters of general coarse microspheres and Fe_3O_4@SiO_2 microspheres.

Symbol	Physical meaning	General coarse microspheres	Fe_3O_4@SiO_2 microspheres
d	Particle's diameter	300 nm	280 nm
E	Young modulus of asperities	1 GPa	70 GPa
ν	Poisson's ratio of asperities	0.25	0.17
μ	Friction coefficient	$0.2 \sim 3.75$	0.227
M_s	Saturation magnetization	200–366 kA m^{-1}	200 kA m^{-1}
H	Magnetic field strength	34–400 kA m^{-1}	34–171 kA m^{-1}

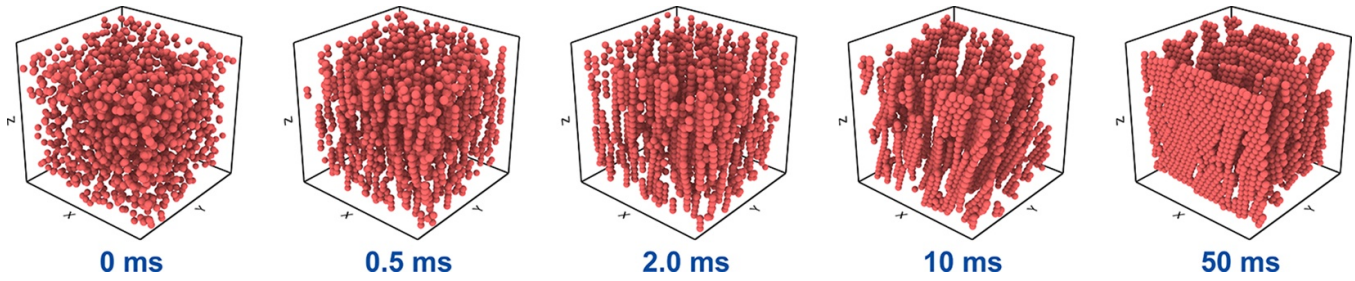

Figure 2. Microstructures of magnetic fluid based on general coarse microspheres at different moments under a uniform magnetic field and steady shear flow. The edge length of the simulation box: 6.13 μm.

The influence of Young modulus on shear stress was discussed in figure 4(b). The Young modulus of magnetic particles was set from 1 to 70 GPa. Here general coarse magnetic microspheres with a saturation magnetization of 200 kA m^{-1} were studied. No significant differences were observed from the curves. The change of E in an order of magnitude did not lead to the deviation of simulation results. Thus, the Young modulus of Fe_3O_4@SiO_2 core–shell microspheres in this work was set as 70 GPa. The Young modulus of pure general coarse magnetic particles was approximated as 1 GPa. Although 1 GPa was not the exact value measured in experiments, this approximation was still reasonable.

3.2. *Effect of friction force in MR properties*

3.2.1. Under a medium friction coefficient. This work was aimed at revealing the correlation between friction force and MR effect from the point of fundamental research. In this section, the friction coefficient was set as 0.2, 0.3, 0.4, and 0.5 according to the typical values in the literature [46, 47]. The particle concentration, saturation magnetization, magnetic field strength, and shear rate were set at 10 vol%, 200 kA m^{-1}, 34 kA m^{-1}, and 100 s^{-1}, respectively. The shear stress was independent of friction force under a medium surface roughness of $0.2 \leq \mu \leq 0.5$ (figure 5(a)). However, the friction force significantly increased the shear stress of non-magnetic particle suspensions with the same friction coefficient [31]. Lobry found that interparticle normal force and tangential force both gave a great contribution to viscosity in a suspension of polystyrene spheres[46]. Singh's simulation revealed that friction force caused a large increase in shear viscosity of concentrated non-magnetic particle suspension [47]. This was because the magnetic dipolar force dominated the rheological behaviors in magnetic fluid, while the extrusion force was the main interaction in non-magnetic particle suspensions. Furthermore, the concentration of particles in non-magnetic particle suspensions, such as shear thickening fluid, could reach as high as $\varphi > 50$ vol% [48]. The volume fraction of magnetic fluid in experiments and applications was usually in the range between 10‘and 30 vol% [49, 50]. Lower concentration brought less extrusion interaction between particles, and further weakened the influence of friction force on the MR effect.

According to equation (13), the shear stress was generated by three kinds of interparticle forces: magnetic force (including van der Waals force), elastic normal force, and friction force. The contribution of each part to shear stress was separately plotted in figure 5(b). Shear stress caused by magnetic force linearly increased to 186 Pa in the first 10 ms of simulations and then fell back. The average contribution from 25 to 50 ms was 60.6 Pa. The elastic normal force gave a negative contribution to shear stress until 30 ms. The largest contribution was −42.6 Pa. The formation and inclination of chain-like microstructures generated strong extrusion between particles. The force equilibrium was mainly the balance between magnetic force and extrusion interaction. The direction of normal force was approximately opposite to the magnetic force and thus generated negative shear stress. After 30 ms, the shear stress originated from normal force fluctuated around zero. The normal extrusion hardly influenced the rheological properties in dynamic equilibrium. Shear stress generated by friction force ranged from −4.71 to 3.91 Pa. The average contribution was 1.62 Pa, two orders of magnitude smaller than the maximum contribution of the magnetic force. This phenomenon was consistent with the results in figure 5(a). According to equation (7), the scale of friction force was an order of magnitude smaller than the normal force. The phenomenon that the contribution of friction force fluctuated around 0 reflected the irregular direction of friction forces

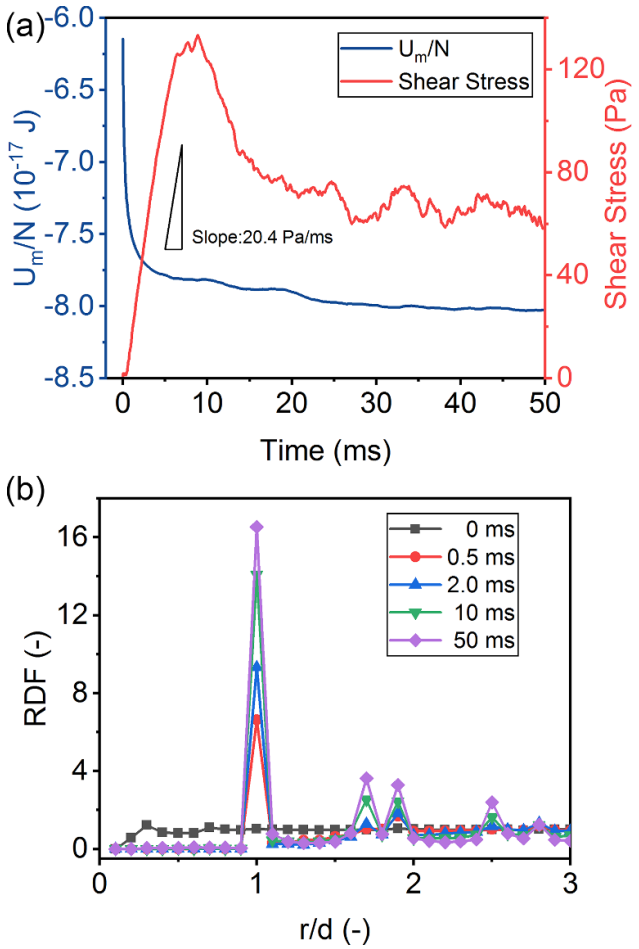

Figure 3. (a) The magnetic potential energy per particle and shear stress versus time. (b) Radial distribution functions at different moments.

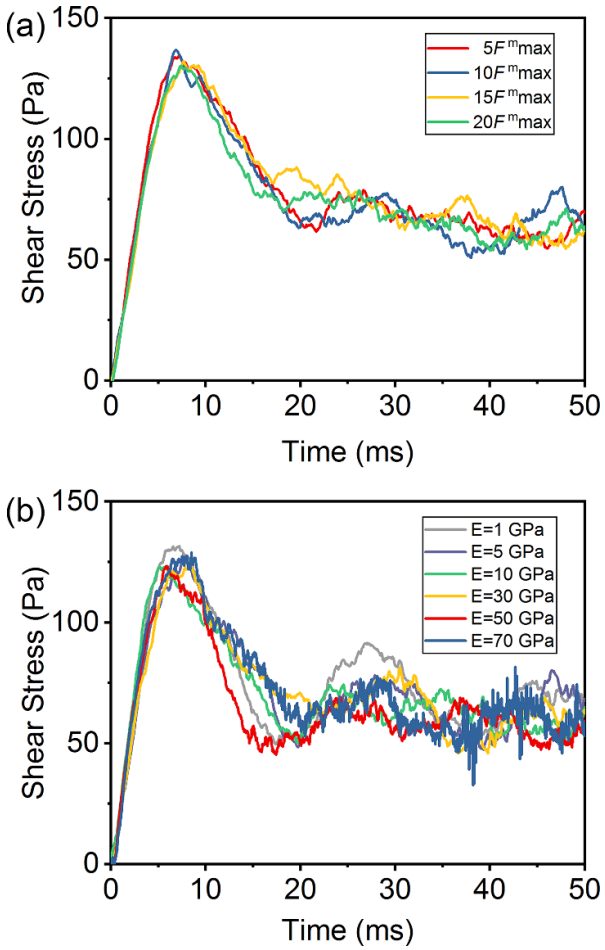

Figure 4. (a) Effect of the upper limit of normal force and (b) Young modulus on shear stress of magnetic fluid.

between particles. From the point of statistical average, friction gave no contribution to shear stress.

3.2.2. Under a large friction coefficient. The microstructures and shear stress of magnetic fluid under a large friction coefficient was simulated in this section. The particle concentration, saturation magnetization, and shear rate were maintained at 10 vol%, 200 kA m^{-1}, and 100 s^{-1}. Two representative magnetic field strengths: 34 and 171 kA m^{-1} were chosen as samples. For magnetic particles with such a saturation magnetization, an external field of 171 kA m^{-1} was very close to the saturation region. Under a strong external field, the friction force still presented no effect on shear stress when $\mu \leq 1.5$ (figure 6(a)). Once the friction coefficient reached the region of $1.5 < \mu < 2.75$, the shear stress fluctuated at a high level after the yield point, which was substantially deviated from figure 5(a). When $\mu = 2.5$, the shear stress generated by magnetic force, elastic normal force, and tangential force was compared in figure 6(b). Shear stress caused by the magnetic force still linearly increased and fluctuated at a high level after the yielding point. The elastic normal force always gave a negative contribution to shear stress and reached a plateau after the yielding. The contribution of the friction force was still close to zero. Figure 6(c) showed the average shear stress was improved by 102% (from 124 to 251 Pa). The maximum shear stress was observed when $\mu = 2.5$. If the friction coefficient further increased, shear stress dropped back to 124 Pa. Under a weak field, the improvement of shear stress was only 24% (from 66 to 82 Pa). But the optimal friction coefficient $\mu = 2.5$ was not influenced by magnetic field strength.

This dramatic increase in shear stress was originated from the particular aggregation of magnetic particles. Microstructures of magnetic fluid with a medium and large friction coefficient were compared in figure 7. Plate-like aggregations were observed at the end of simulations when $\mu = 0.5$. There was more space between the plates compared to the microstructures when $\mu = 0.27$ (figure 2). However, inclined thick chain-like microstructures were always obtained when $\mu = 2.5$. The different thickness of microstructures was obvious in the top view (figure 7(a)). Once the magnetic fluid reached the yield point, single-particle-width chains were destroyed by the shear flow. The flow of the matrix also created opportunities for the broken chains to contact each other along the x-axis. As a result, single-particle-width chains merged into inclined thick chains. Then, two thick chains were analyzed from the top view (figure 7(c)). The front chain imposed a magnetic attraction on each particle

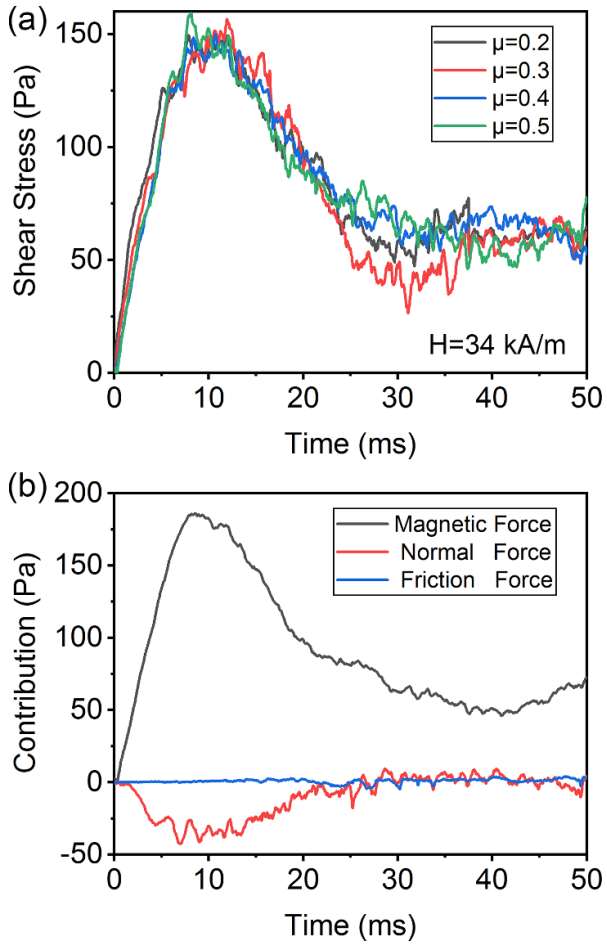

Figure 5. (a) Shear stress versus time curves of magnetic fluid based on general coarse magnetic microspheres with different friction coefficients. (b) The contribution of inter-particle magnetic force, normal force, and friction force to shear stress when $\mu = 0.5$.

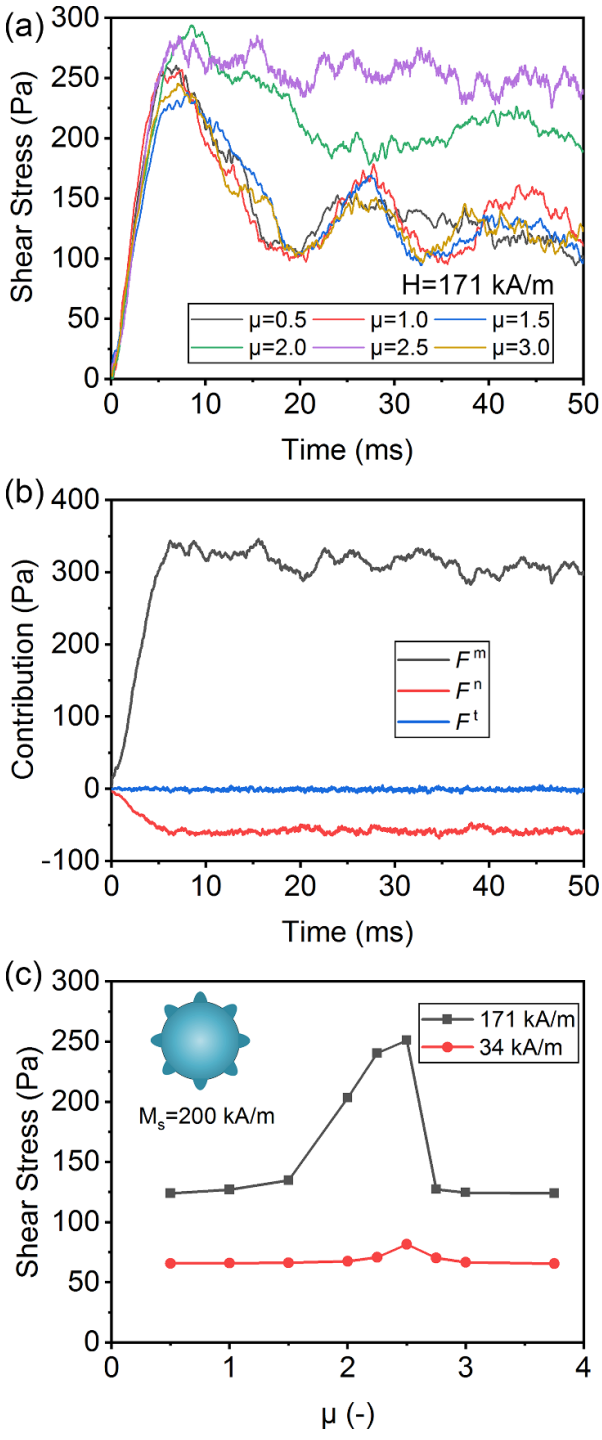

Figure 6. (a) Shear stress versus time of magnetic fluid based on general coarse magnetic microspheres under large interparticle friction coefficients, $H = 171$ kA m^{-1}. (b) Contribution of magnetic force, normal force, and tangential force to shear stress when $\mu = 2.5$. (c) Average shear stress versus friction coefficient under different magnetic fields. Inset: illustration of general coarse magnetic microspheres, the asperities on the surface were not plotted in scale.

in the rear chain. The particles on the edge of the rear chain experienced a weaker magnetic force than those in the center due to the larger distance from the front chain. The magnetic attraction also possessed a y-component as a result of the relative direction between particles. Under a small friction coefficient, particles on the edge gradually moved along the y-axis and formed plate-like microstructures. Under a large friction coefficient, the magnetic dipolar force along the shear direction cannot overcome strong friction interactions. The movement of particles along the y-axis and the formation of plate-like microstructures were blocked. The larger dip angle of thick chain structures resulted in larger shear stress. In summary, the influence of friction coefficient on microstructures was relevant to the relative strength between magnetic dipolar force and friction interaction. The break-up and reformation of thick chains led to the fluctuation of shear stress at a high level. If μ exceeded 2.5, the aggregation along the field direction was also hindered. Long chains were replaced by short ones, which led to a decrease in shear stress

The contribution of interparticle magnetic force, elastic normal force, and friction force to shear stress when $\mu = 2.5$ was discussed in figure 6(b). Although the friction forces were quite strong, its contribution to shear stress was still close to zero. The increasing friction coefficient greatly changed the aggregation of particles. But the friction force only gave a small direct contribution to shear stress, which was the same

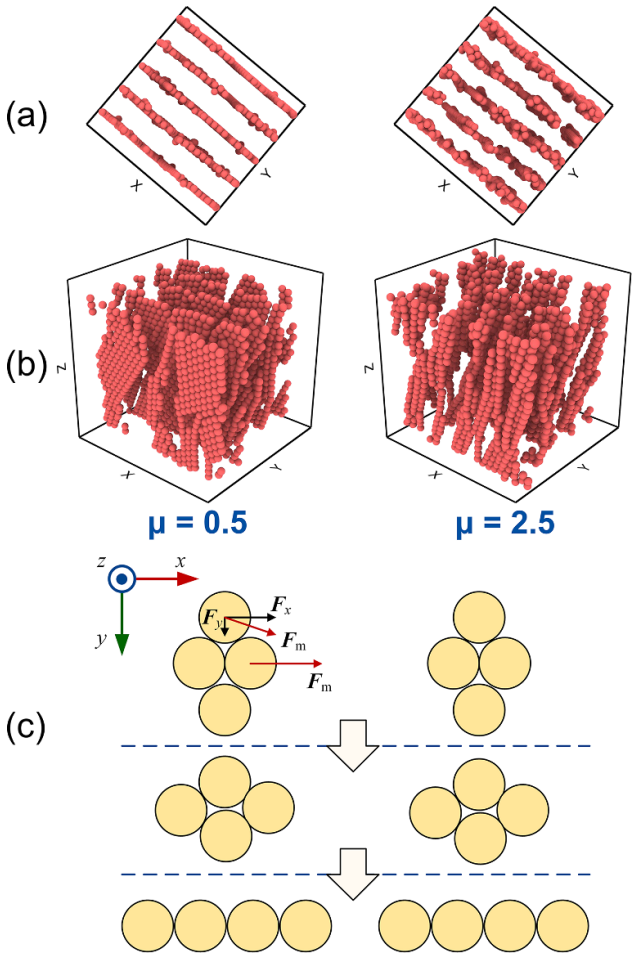

Figure 7. Microstructures of magnetic fluid with different friction coefficients at the end of simulations, (a) top view and (b) perspective view. (c) Schematic diagram of the evolution from thick chains to plate-like microstructures.

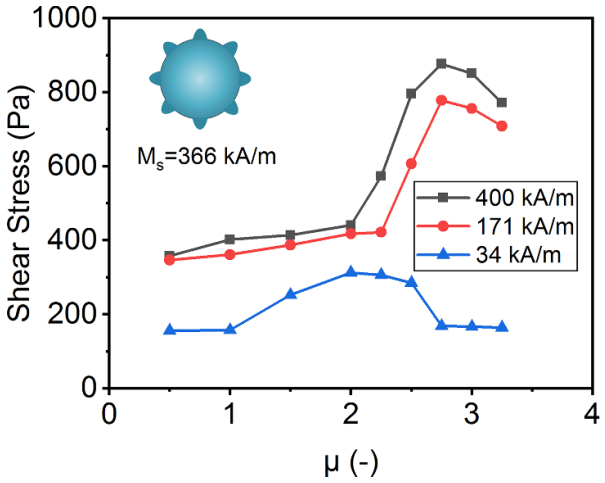

Figure 8. Average shear stress of magnetic fluid based on general coarse microspheres versus friction coefficient under a weak, medium, and saturated magnetic field. Inset: illustration of general coarse magnetic microspheres, the asperities on the surface were not plotted in scale.

as figure 4(b). It was the magnetic force among particles who generated strong shear stress and improved the MR effect under such a situation. In other words, the interparticle friction force indirectly enhanced the MR effect.

The trend of shear stress versus friction coefficient and the optimal friction coefficient under different saturation magnetizations, external fields, shear rates, and particle concentrations were then simulated. The surface roughness of magnetic particles could be modified according to the working conditions to achieve the best MR effect.

If the saturation magnetization of general coarse magnetic microspheres was increased to 366 kA m^{-1}, the relationship between shear stress and friction coefficient was also investigated. Here the external fields were chosen as 34, 171, and 400 kA m^{-1}. Generally speaking, the larger saturation magnetization of particles, the stronger external field was required to reach saturation. The last magnetic induction could ensure the particles in the saturation state. The particle concentration and shear rate were set at 10 vol%, and 100 s^{-1}. Figure 8 indicated the shear stress under different friction coefficients was always enhanced with the increasing external field. The improvement of shear stress caused by interparticle friction forces also exhibited the same trend. The optimal μ was 2.0 under a 34 kA m^{-1} magnetic field and increased to 2.75 when the external field reached 171 kA m^{-1}. This value remained unchanged after magnetic saturation.

If the saturation magnetization increased, the y-component of magnetic dipolar force was enhanced due to the larger magnetic moments. This non-uniform magnetic attraction was also in proportion to the magnetic field strength. The difference in magnetic dipolar forces under various external fields became more obvious than the situation of lower saturation magnetization. Particles on the edge of the thick chains experienced stronger driving forces to form plate-like microstructures (figure 7(c)). To improve the MR effect, the interparticle friction should be increased to hinder the aggregation of particles. Thus the optimal μ increased with the external field and finally exceeded the value when $M_s = 200$ kA m^{-1}. The y-component of magnetic dipolar force saturated if $H = 400$ kA m^{-1}, thus the optimal μ did not further increase.

The trend of shear stress versus friction coefficient under different shear rates and particle concentrations were simulated at last. The saturation magnetization and external field strength were 366 and 171 kA m^{-1}. If the shear rate increased from 60 to 100 s^{-1}, the maximum shear stress was improved from 714 to 778 Pa, while the optimal $\mu = 2.75$ remained unchanged (figure 9(a)). Single-particle-width chains were easily destroyed under a large shear rate. The evolution of microstructures became faster with the increasing velocity of the matrix. Furthermore, the inclinations of plate-like microstructures and thick chains also increased when increasing the shear rate. Microstructures with a larger dip angle generated stronger x-component of magnetic dipolar forces between particles to resist the shear flow. Therefore, the shear stress improved with the increasing shear rate. However, the change of shear rate did not influence the relative strength between magnetic dipolar force and friction interaction. The trend of shear

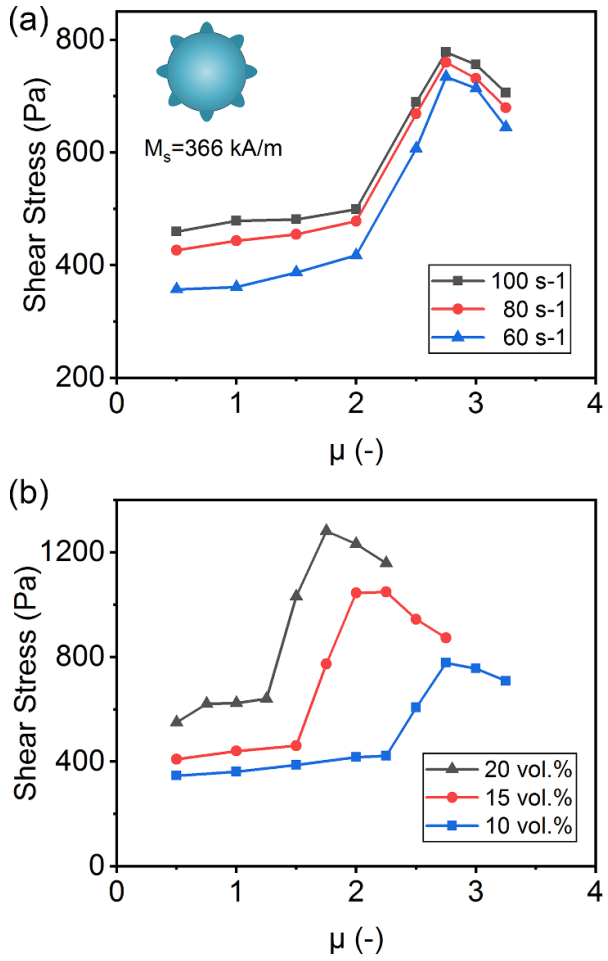

Figure 9. (a) Average shear stress versus friction coefficient curves of magnetic fluid based on general coarse magnetic microspheres under different shear rates, $\varphi = 10$ vol%; (b) under different particle concentrations, $\dot{\gamma} = 100\ s^{-1}$. Inset: illustration of general coarse magnetic microspheres, the asperities on the surface were not plotted in scale.

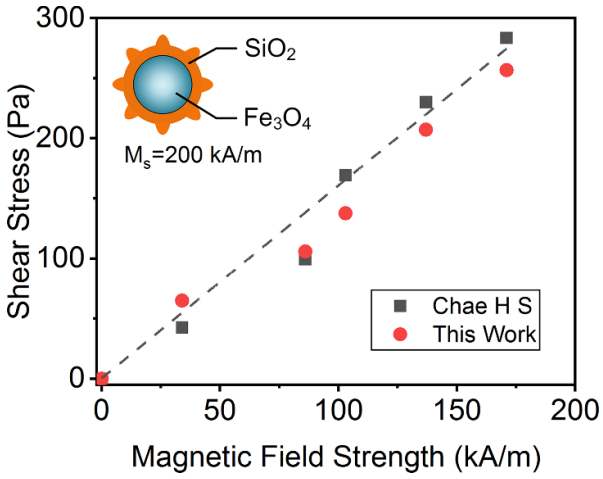

Figure 10. Comparison of simulated and experimental shear stress of Fe_3O_4@SiO_2 magnetic fluid in magnetic field sweep, $\dot{\gamma} = 100\ s^{-1}$. Inset: illustration of Fe_3O_4@SiO_2 microspheres, the asperities on the surface were not plotted in scale.

stress versus friction coefficient was independent of the shear rate. When the particle volume fraction increased from 10 to 20 vol%, the maximum shear stress increased from 778 to 1281 Pa. The optimal μ decreased from 2.75 to 1.75 (figure 9(b)). Although the total magnetic force imposed on each coarse magnetic microsphere was strengthened with the increasing volume fraction. But the high concentration also created a lot of contact opportunities between particles and greatly enhanced the extrusion and friction forces. The effect of friction force on shear stress was determined by the competition between magnetic force and friction interaction. Only a small friction coefficient was required to improve the MR effect in concentrated suspensions.

3.3. Experimental verification

To verify the accuracy of this work, the shear stress in magnetic field sweep of an existing magnetic fluid, the Fe_3O_4@SiO_2 magnetic fluid, was simulated and compared to experiments. The physical properties of particles and simulation parameters were set the same as the literature [29]. Figure 10 indicated that simulation results were very close to experiments. Shear stress presented a linear dependence on the magnetic field strength with a slop of 1.6 Pa m kA^{-1}. Some deviations from the experiments were observed when the magnetic field was around 100 kA m^{-1}. The experimental data points were measured from Chae's work by using the Origin software [29]. The figure recognizing process of the software might bring some errors in experimental shear stress. The error of simulations was originated from the limit of the simulation scale. The influence of large-scale particle aggregations on shear stress was not considered due to limited computer performance. More effort will be put to investigate this issue in the future.

4. Conclusion

In conclusion, the influence of interparticle friction on the MR effect of magnetic fluid was studied using modified particle-level dynamic simulations. The friction coefficients greatly influenced the microstructures of magnetic fluid and improved the shear rheological properties. Under a moderate friction force ($0.2 \leq \mu \leq 1.5$), plate-like microstructures were formed in the homeostasis of magnetic fluid. Shear stress was independent of the friction coefficient, which was due to the low particle concentration and irregular direction of friction forces. Under a large friction coefficient ($\mu > 1.5$), particles always aggregated into inclined thick chains. The MR effect could be improved by 102% in steady shear flow. Friction forces restricted the relative movement of particles in the thick chains and hampered the formation of plate-like microstructures. Thick chains possessed larger dip angles than plate-like microstructures. Interparticle magnetic forces generated strong shear stress under such a situation. The enhancement of shear stress was relevant to the relative strength between magnetic force and friction interaction. The optimal friction coefficient under

different saturation magnetizations, external fields, shear rates, and particle concentrations were determined by simulations. The surface roughness of magnetic particles could be modified according to the working conditions to achieve the best MR effect. When $M_s = 200$ kA m^{-1}, the optimal $\mu = 2.5$ was independent of the external field. If $M_s = 366$ kA m^{-1}, the optimal μ increased from 2 to 2.75 with the increasing magnetic field strength until saturation. The optimal friction coefficient was not influenced by the shear rate, while this value decreased with the increasing particle concentrations. Finally, simulated shear stress of an existing Fe_3O_4@SiO_2 magnetic fluid matched well with experiments. This work promoted the comprehension of MR mechanism and provided suggestions for the preparation of high-performance magnetic fluid. Future work would be aimed at further improving the accuracy of simulations and investigating the influence of interparticle friction on the electric conduction of magnetic fluid.

Acknowledgments

This work is supported by the National Natural Science Foundation of China (Grant No. 11822209). The Joint Fund of USTC-National Synchrotron Radiation Laboratory (KY2090000055) is gratefully acknowledged.

ORCID iD

Xinglong Gong https://orcid.org/0000-0001-6997-9526

References

[1] De Vicente J, Klingenberg D J and Hidalgo-Alvarez R 2011 *Soft Matter.* **7** 3701–10
[2] Tran V T, Zhou H J, Lee S, Hong S C, Kim J, Jeong S Y and Lee J 2015 *ACS Appl. Mater. Interfaces* **7** 8650–8
[3] Park I H and Choi H J 2018 *J. Ind. Eng. Chem.* **64** 102–6
[4] Vekas L 2009 *Adv. Sci. Tech.* **54** 127–36
[5] Sun S S, Yang J, Li W H, Du H, Alici G, Yan T H and Nakano M 2017 *Mech. Syst. Signal Process.* **83** 371–84
[6] Yang J, Sun S S, Ning D, Li Z, Deng L, Christie M D, Du H, Zhang S W and Li W H 2019 *Smart Mater. Struct.* **28** 105003
[7] Yang M D, Ho C H, Ruta S, Chantrell R, Krycka K, Hovorka O, Chen F R, Lai P S and Lai C H 2018 *Adv. Mater.* **30** 1802444
[8] Tay Z W *et al* 2018 *ACS Nano* **12** 3699–713
[9] Xing Z W, Yu M, Sun S S, Fu J and Li W H 2016 *Smart Mater. Struct.* **25** 015026
[10] Yazid I I M, Mazlan S A, Imaduddin F, Zamzuri H, Choi S B and Kikuchi T 2016 *Smart Mater. Struct.* **25** 125005
[11] Prozorov T, Prozorov R and Gedanken A 1998 *Adv. Mater.* **10** 1529
[12] Fang Q L, Zhang J F, Bai L F, Duan J Y, Xu H J, Leung K C F and Xuan S H 2019 *J. Hazard Mater.* **367** 15–25
[13] Lópe-Lópe M T, Kuzhir P and Bossis G 2009 *J. Rheol.* **53** 115–26
[14] Vereda F, Segovia-Gutierrez J P, de Vicente J and Hidalgo-Alvarez R 2016 *Appl. Phys. Lett.* **108** 211904
[15] Li W H and Zhang X Z 2008 *Korea-Aust. Rheol. J.* **20** 45–50 (https://ro.uow.edu.au/engpapers/3910)
[16] Laherisheth Z and Upadhyay R V 2017 *Smart Mater. Struct.* **26** 054008
[17] Tong Y, Dong X F and Qi M 2017 *Smart Mater. Struct.* **26** 025023
[18] Vereda F, de Vicente J, Segovia-Gutierrez J P and Hidalgo-Alvarez R 2011 *J. Phys. D: Appl. Phys.* **110** 063520
[19] Siebert E, Laherisheth Z and Upadhyay R V 2015 *Smart Mater. Struct.* **24** 075011
[20] Liu M 1995 *Phys. Rev. Lett.* **74** 4535–8
[21] Wang Z, Shahrivar K and de Vicente J 2014 *J. Rheol.* **58** 1725–50
[22] Warnke W C 2003 *IEEE Trans. Magn.* **39** 1771–7
[23] Mousavi S M, Darzi A A R, Akbari O A, Toghraie D and Marzban A 2019 *J. Magn. Magn. Mater.* **473** 42–50
[24] Klingenberg D J, Vanswol F and Zukoski C F 1989 *J. Chem. Phys.* **91** 7888–95
[25] Ruiz-López J A, Wang Z W, Hidalgo-Alvarez R and de Vicente J 2017 *J. Rheol.* **61** 871–81
[26] Ruiz-López J A, Wang Z W, Fernandez-Toleda J C, Hidalgo-Alvarez R and de Vicente J 2016 *Rheol. Acta.* **55** 245–5
[27] Pei L, Xuan S H, Wu J, Bai L F and Gong X L 2019 *Langmuir* **35** 12158–67
[28] De Vicente J and Ramírez J 2007 *J. Colloid Interface Sci.* **316** 867–76
[29] Chae H S, Kim S D, Piao S H and Choi H J 2016 *Colloid Polym. Sci.* **294** 647–55
[30] Blanc F, Peters F and Lemaire E 2011 *Phys. Rev. Lett.* **107** 208302
[31] Peters F, Ghigliotti G, Gallier S, Blanc F, Lemaire E and Lobry L 2016 *J. Rheol.* **60** 715–32
[32] Kim K H, Kim M J, Choa Y H, Kim D H and Yu J H 2008 *IEEE Trans. Magn.* **44** 2940–3
[33] Liu T X, Gong X L, Xu Y G, Xuan S H and Jiang W Q 2013 *Soft Matter.* **9** 10069–80
[34] Pei L, Pang H M, Chen K H, Xuan S H and Gong X L 2018 *Soft Matter.* **14** 5080–91
[35] Faure B, Salazar-Alvarez G and Bergström L 2011 *Langmuir* **27** 8659–64
[36] Klingenberg D J, Olk C H, Golden M A and Ulicny J C 2010 *J. Phys.: Condens. Matter.* **22** 324101
[37] Gallier S, Lemaire E, Peters F and Lobry L 2014 *J. Fluid Mech.* **757** 514–49
[38] Wu A Z, Shi X and Polycarpou A A 2012 *J. Appl. Mech.* **79** 051001
[39] Brizmer V, Kligerman Y and Etsion I 2007 *Tribol. Lett.* **25** 61–70
[40] He L, Tafti D K and Nagendra K 2017 *Powder Technol.* **313** 332–43
[41] Shahrivar K, Morillas J R, Luengo Y, Gavilan H, Morales P, Bierwisch C and de Vicente J 2019 *J. Rheol.* **63** 547–58
[42] Deulin E A, Gatsenko A A and Loginov B A 1999 *Surf. Sci.* **433** 288–92
[43] Kim M T 1996 *Thin Solid Films* **283** 12–16
[44] Jang J S, Kim H I, Gibson R F and Suhr J 2013 *Mater. Des.* **51** 219–24
[45] Stukowski A 2009 *Simul. Mater. Sci. Eng.* **18** 015012
[46] Lobry L, Lemaire E, Blanc F, Gallier S and Peters F 2019 *J. Fluid Mech.* **860** 682–710
[47] Singh A, Mari R, Denn M M and Morris J F 2018 *J. Rheol.* **62** 457–68
[48] Cao S S, He Q Y, Pang H M, Chen K H, Jiang W Q and Gong X L 2018 *Smart Mater. Struct.* **27** 085013
[49] Ruan X H, Pei L, Xuan S H, Yan Q F and Gong X L 2017 *J. Magn. Magn. Mater.* **429** 1–10
[50] Ruan X H, Xuan S H, Zhao J, Bian H T and Gong X L 2020 *Smart Mater. Struct.* **29** 055018